Available online at www.sciencedirect.com

SciVerse ScienceDirect

Ceramics International 39 (2013) 1885–1892

CERAMICS INTERNATIONAL

www.elsevier.com/locate/ceramint

High supercapacitive stability of spray pyrolyzed ZnO-added manganese oxide coatings

Chin-Yi Chen[a,*], Hung-Wei Chang[a], Shao-Ju Shih[b], Chien-Yie Tsay[a], Chi-Jung Chang[c], Chung-Kwei Lin[d]

[a]Department of Materials Science and Engineering, Feng Chia University, 100, Wenhwa Road, Seatwen, Taichung 40724, Taiwan, ROC
[b]Department of Materials Science and Engineering, National Taiwan University of Science and Technology, 43, Sect. 4, Keelung Road, Da'an, Taipei 10607, Taiwan, ROC
[c]Department of Chemical Engineering, Feng Chia University, 100, Wenhwa Road, Seatwen, Taichung 40724, Taiwan, ROC
[d]Department of Dentistry, Taipei Medical University, 250, Wu-Hsing Street, Sinyi, Taipei 11031, Taiwan, ROC

Received 9 May 2012; received in revised form 11 August 2012; accepted 13 August 2012
Available online 21 August 2012

Abstract

Zinc oxide (ZnO) has recently been reported to exhibit electrochemical supercapacitive properties. We demonstrate, for the first time, a nanocrystalline (< 10 nm) composite powder electrochemical supercapacitor in which ZnO-added manganese oxide is used as the active electrode material. The ZnO-added (≤ 10 at%) manganese oxide powders were prepared from their acetate-based salts by spray pyrolysis (SP) at 500 °C and subsequently coated onto graphite substrates by electrophoretic deposition (EPD) to produce supercapacitor electrodes. XRD data and TEM observation identified the ZnO-added manganese oxide as tetragonal Mn_3O_4 phase with a nanocrystalline structure. ZnO may dissolve in manganese oxide and inhibit the grain growth of the manganese oxide. Cyclic voltammetry showed that the specific capacitance (SC) of the manganese oxide coating in 1 M Na_2SO_4 electrolyte increased from 196 F/g to 230 F/g at 25 mV/s for 5 at% ZnO-added manganese oxide. After activation, the cycling efficiency of the composite electrode exhibited a high value of $> 90\%$ for up to 1200 cycles for all the compositions.
© 2012 Elsevier Ltd and Techna Group S.r.l. All rights reserved.

Keywords: Electrophoretic deposition; Manganese oxide; Spray pyrolysis; Zinc oxide

1. Introduction

Electrochemical capacitors, which have recently attracted R&D attention due to their high power density and high energy density, can be used for hybrid power applications requiring a high power output and/or a high cycle capacity, such as uninterruptible power supply units for computers, power electronics, and electric vehicles [1–3]. According to the charge storage mechanisms, electrochemical capacitors can be classified into two categories: electric double-layer capacitors (EDLCs) and reversible faradaic reaction of metal oxides (pseudocapacitors) [4,5]. The EDLC consists of a high specific surface material, such as activated carbon or carbon aerogel, which stores physically the electronic or ionic charges by double-layer formation at the electrode/electrolyte interfaces. However, the pseudocapacitor consists of a metal oxide such as RuO_2, MnO_2, IrO_2, or ZnO, which have various oxidation states and can store electronic or ionic charges not only by physical adsorption but also by reversible faradaic redox reaction occurring on the electrode surface. Therefore, the pseudocapacitor is a promising device due to its relatively fast and reversible faradaic redox reactions.

Among metal oxides, hydrous ruthenium oxide electrode has been reported to have an extremely high SC value of 720 F/g in aqueous H_2SO_4 and excellent reversibility [6,7]; however, it is expensive and toxic. Manganese has various oxidation states and complex structures, and it is lower in cost and more environmentally friendly than other transition

*Corresponding author. Tel.: +886 4 24517250; fax: +886 4 24510014.
E-mail address: chencyi@fcu.edu.tw (C.-Y. Chen).

0272-8842/$ - see front matter © 2012 Elsevier Ltd and Techna Group S.r.l. All rights reserved.
http://dx.doi.org/10.1016/j.ceramint.2012.08.037

metal oxides. Hence, Mn-oxide based supercapacitors have recently received much attention in R&D in energy-related fields. Amorphous hydrous Mn-oxide (a-$MnO_2 \cdot nH_2O$) has recently been reported to be a promising supercapacitor electrode material because its SC value is higher than that of crystalline MnO_2 [8–11]. Therefore, we used an SP technique to react the metal salts into metal oxides by using temperatures that yield homogeneous metal oxides with various amounts of amorphous and/or hydrous residuals.

In our previous studies [12–14], we have demonstrated that Mn-oxide electrode can be prepared by a combination of SP and EPD techniques. Furthermore, zinc oxide (ZnO), which has several excellent physical properties, has been applied in electronic and optoelectronic devices [15–17]. However, available information on the suitability of ZnO as a potential candidate for supercapacitor application is still very limited [18]. To the best of our knowledge, although carbonaceous material/ZnO composite has been demonstrated to exhibit high SC values [19,20], a MnO_x/ZnO composite fabricated for supercapacitor electrode has not yet been reported. In this research, various amounts of zinc ion were directly added into the precursor solution to synthesize homogeneous ZnO-added Mn-oxide powders via SP. The morphological and structural characteristics of the resulting powder were investigated by transmission electron microscopy (TEM) and X-ray diffractometry (XRD). The as-pyrolyzed powders were then coated onto graphite substrates by EPD. The pseudocapacitive properties and the cycling stability of SP Mn-oxide powder as a function of Zn addition were examined.

2. Experimental

Manganese oxide powders with various amounts of ZnO addition (0, 1, 2, 5, and 10 at%) were homogeneously synthesized using an SP/ESD (electrostatic deposition, for powder collection) system. Details of the experimental set-up are described elsewhere [12,13]. The precursors used for generation of Mn/Zn oxide powders in this study were manganese acetate (MnA) and zinc acetate dihydrate (ZnA). The chemical formulas of MnA and ZnA are $Mn(CH_3COO)_3 \cdot 2H_2O$ (ProChem Inc., USA) and $Zn(CH_3COO)_2 \cdot 2H_2O$ (Showa, Japan), respectively. These chemicals are both reagent grade with 99.0% purities. The precursor solutions, MnA or (MnA + ZnA) in de-ionized water, were prepared as 0.5 wt%. The reaction temperature was set at 500 °C for powder formation (the product powders pyrolyzed at 500 °C are denoted as SP500).

The as-prepared powders were electrophoretically deposited onto graphite substrates ($10 \times 10\ mm^2$) for characterization of electrochemical properties. Details of the EPD process were described in a previous study [13]. The morphology and phase of SP powder were examined using transmission electron microscopy (1200EX, JEOL II, Japan) and X-ray diffractometry (SRA-M18XHF MAC Science, Japan), respectively. Electrochemical properties of the deposited powder coatings were analyzed in a three-compartment cell by an electrochemical analyzer system (CH Instruments, Model 727C, USA). An Ag/AgCl electrode was used as the reference electrode, and a piece of graphite served as the counter electrode. The morphologies of the EPD particle coatings before and after CV were observed by scanning electron microscopy (SEM, JSM-6700F, JEOL, Japan). The specific surface areas of the as-pyrolyzed powders were determined by the BET (Brunauer–Emmer–Teller) method from nitrogen adsorption and desorption isotherm data obtained at −196 °C on a constant-volume adsorption apparatus (SA-9600 Series, HORIBA, Japan).

3. Results and discussion

According to our previous thermogravimetry data, the precursor MnA, when heated at a temperature higher than 400 °C, decomposes into Mn-oxide [13,14]. Therefore, in this study, the reaction temperature was set at 500 °C for the formation of the ZnO-added SP500 powder. Fig. 1 shows XRD patterns of the as-obtained powders from the spray pyrolyzed MnA and (MnA + ZnA) precursor solutions at 500 °C as a function of ZnO content. It can be noted that all the resulting powders were identified as a phase of tetragonal Mn_3O_4 with broadened diffraction peaks, indicating poor crystallinity. This was expected, since a residual amorphous phase, particularly on the surface, is usually found in wet-chemical synthesis. However, weak signals of ZnO phase can be noticed in the XRD patterns. We suspect that these can be attributed to the dissolution of the zinc in the Mn-oxide matrix [21,22] and the small amount of zinc addition. Moreover, estimation of the crystallite size of the ZnO-added SP500 powders by Scherrer formula revealed a nanocrystalline structure with a crystallite size of < 10 nm, as shown in Fig. 2. The figure shows the crystallite size and lattice volume of SP500 powders as a function of ZnO addition. The respective crystallite sizes of the SP500 powders were calculated to be 9.3, 10.2, 8.4, 8.0 and 7.9 nm for 0, 1, 2, 5 and 10 at% zinc additions, respectively. The crystallite size of SP500 powder increased slightly when 1 at% zinc was added, and then decreased with larger additions of ZnO. The crystallite size of SP500 powder was increased by the addition of a small amount of ZnO, suggesting the dissolution of ZnO in the Mn-oxide matrix. With greater additions of ZnO, the crystallite size of the pyrolyzed Mn-oxide powder decreased, possibly due to the inhibition effect of excess Zn ions. Similar results were also found in an SP NiO-added YDC (yttria-doped ceria) system in our previous study [23].

Fig. 3 shows TEM micrographs of the as-obtained unadded and 5 at% ZnO-added Mn-oxide particles synthesized by SP at 500 °C. It was expected that particles pyrolyzed from the MnA precursor would have a rounded shape with uneven surfaces. The hollow structure of some particles was attributed to surface precipitation of the MnA precursor during SP [13]. A similar particle

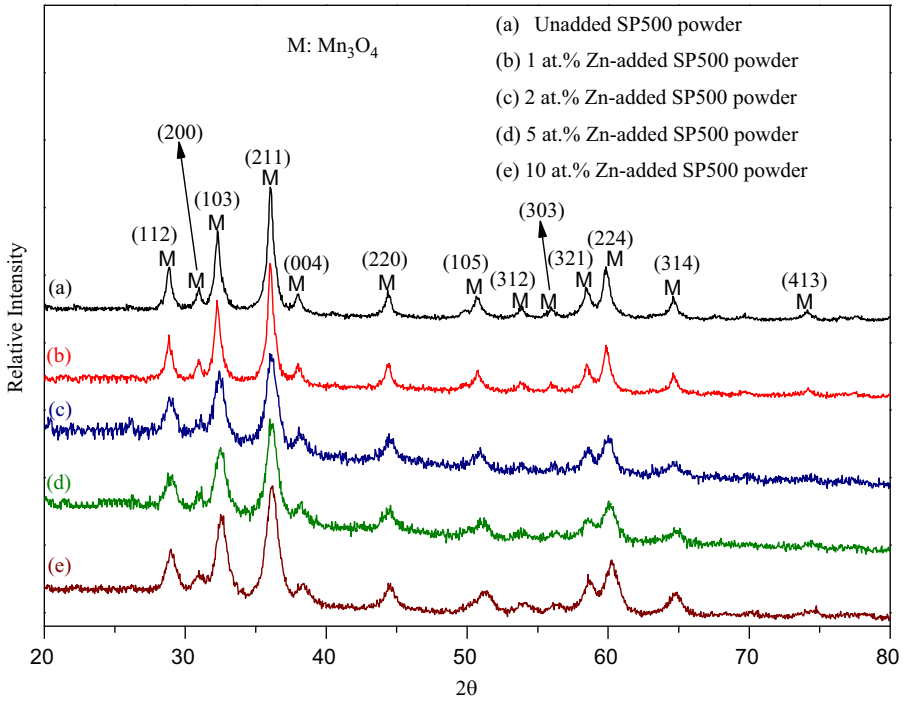

Fig. 1. XRD patterns of as-pyrolyzed SP500 powder as a function of ZnO addition.

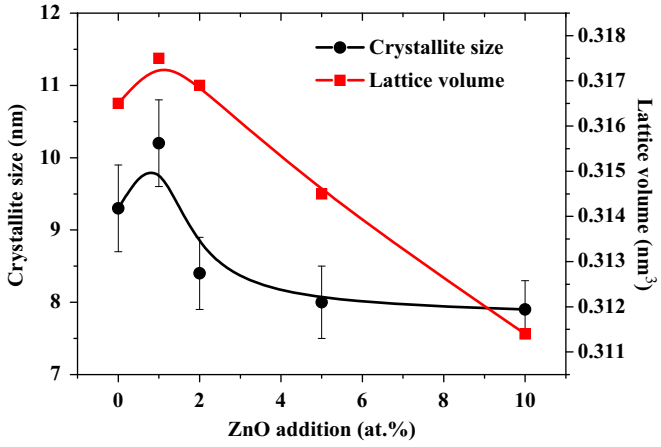

Fig. 2. Crystallite size and lattice volume of SP500 powder as a function of ZnO addition.

morphology can be found in the ZnO-added equivalent. However, a larger amount of fragments was noticed in ZnO-added SP500 powders. This increased number of fragments is attributed to the shrinkage of the hollow particles during cooling in SP. Some shriveled particles also resulted, as shown in both micrographs. Zinc oxide addition seems to increase the fragility of the SP500 particle shell. Unable to tolerate significant deformation, the shells of some of the larger particles fractured. Moreover, crystallites on the shells of the particles were found to be very fine, with a size of < 10 nm. Such a fine crystallite

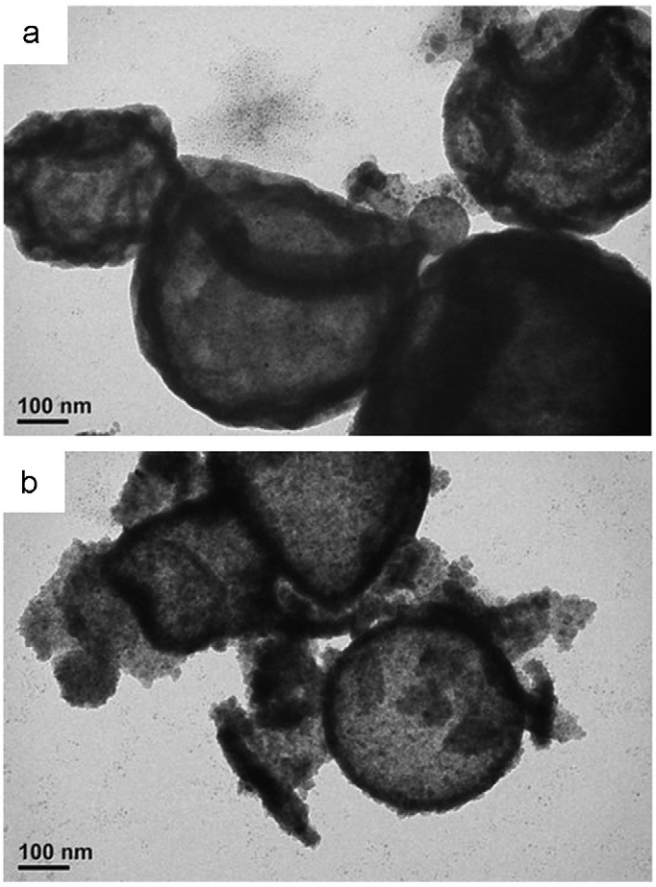

Fig. 3. TEM micrographs of as-pyrolyzed (a) unadded and (b) 5 at% ZnO-added SP500 powders.

size can also be determined from the magnified TEM micrographs (not shown here), confirming the results calculated by Scherrer formula from the XRD patterns. The respective crystallite sizes were measured to be 9.6, 10.4, 8.6, 8.3 and 8.0 nm for 0, 1, 2, 5 and 10 at% ZnO additions, respectively. These results are consistent with the trend calculated from the XRD data. The values are also quite close to one another.

The as-pyrolyzed SP500 powders were subsequently deposited onto graphite substrates by EPD. The pseudo-capacitive characteristics of the electrophoretically deposited SP powders were analyzed by cyclic voltammograms (CV) and life tests. Fig. 4 shows CV curves of the as-deposited unadded and ZnO-added SP500 powder coatings in 1.0 M Na_2SO_4 in the range of 0–1.0 V with a scan rate of 25 mV/s. The CV curves are almost rectangular in shape, exhibiting a typical capacitive behavior with a charging current in both scanning directions across the potential range of 0–1.0 V. The CV curves also demonstrate that the EPD SP500 powder coatings have good redox reversibility. Moreover, the area under the CV curve can be used to estimate the SC value of the system. The 5 at% ZnO-added SP500 electrode exhibited the largest area, and thus the highest SC in this system. Table 1 shows the SCs measured from the 50th CV cycle at various scan rates for the SP500 powder coating as a function of ZnO addition. Note that all the SCs for the EPD SP500 electrodes decreased with increases in scan rate, revealing the slow diffusion rate of electrolyte ions gaining access to the available sites by intercalation and/or absorption [24]. The higher the scan rate, the lower the measured SC. This effect may become significant when scan rate is slow. Since the small crystallite size can provide a larger number of available sites for ionic intercalation/absorption, the largest crystallite size, found in the 1 at% ZnO-added SP500 powder coating (Fig. 2), exhibits the lowest SC value at a scan rate of 25 mV/s. Moreover, unlike the SC of 1 at% ZnO-added SP500 at a scan rate of 25 mV/s, the SC of the SP500 coating increased when ZnO was added at various scan rates. Referring again to the scan rate of 25 mV/s, the

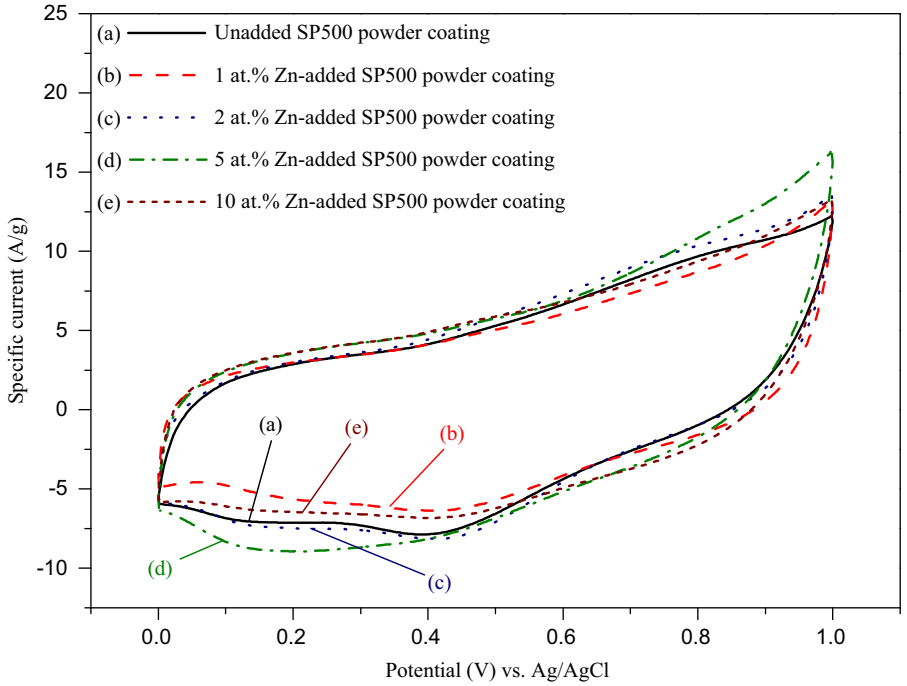

Fig. 4. Cyclic voltammograms of Mn-oxide powder coatings measured from the 50th cycle in 1.0 M Na_2SO_4 electrolyte at a scan rate of 25 mV/s as a function of ZnO addition.

Table 1
Specific capacitance measured from the 50th CV cycle in 1.0 M Na_2SO_4 at various scan rates for SP500 powder coating as a function of ZnO addition.

Scan rate (mV/s)	ZnO addition in SP400 Mn-oxide powder (at%)				
	0	1	2	5	10
	specific capacitance (F/g)				
25	196	183	211	230	206
50	137	142	149	163	161
100	95	109	108	120	126

capacitance increased from 196 F/g to attain its highest value, 230 F/g, when 5 at% of zinc was added, and then decreased to 206 F/g when the zinc addition was increased to 10 at%.

Fig. 5 shows the galvanostatic charge/discharge cycle for the EPD SP500 powder coating in 1.0 M Na_2SO_4 electrolyte at a current of 1.0 M as a function of ZnO addition. The cyclic *E-t* spike of the electrode shows electrochemical reversibility due to the symmetry of the anodic charging curve to its cathodic discharging counterpart. Notice that the curves for the ZnO-added Mn-oxide electrodes have more rapid charge and discharge rates than does that for the unadded one. These higher rates may result from the nonstoichiometric structure of the Zn/Mn oxide solid solution. Though the specific capacitance of electrode can be calculated from the slope of the charge/discharge curve, the significant *i*R drop in both charging and discharging processes of all the SP500 powder electrodes may cause scatter and error in the estimated SC values. Therefore, in this system, the SC values were calculated from the area under the CV curves.

Since the 5 at% ZnO-added SP500 coating exhibited the best electrochemical performance in the present study, further examinations and characterizations focused on corresponding samples. Fig. 6 shows SEM micrographs of the as-deposited unadded and 5 at% ZnO-added SP500 powders. The structure of the particle coating can be seen in the top-view micrographs after EPD. Like the TEM morphology, some larger unadded particles revealed fracture surfaces, as indicated by arrows in Fig. 6(a). The broken particles may expose a large area of the inner structure. However, particles in 5 at% ZnO-doped SP500 powder coating, shown in Fig. 6(b), became more irregular and fragmented, though some particles still remained on/in the coating after EPD.

Research indicates that the electrochemical characteristics of electrode materials are highly dependent on the grain size, texture, surface area, and morphology. We believe that the surface of the powder coatings may indeed influence their capacitive performance. Because it was extremely difficult to measure the surface area of the powder coatings in experiments, we measured the specific surface area of the as-pyrolyzed powders by the BET method. Assuming that each EPD condition was identical, the specific surface areas of the SP powders can be calculated on behalf of the surface areas of their powder coatings for comparison. The specific surface areas of the unadded, 1, 2, 5 and 10 at% ZnO-added SP500 powders were determined to be 26.7, 25.6, 32.0, 44.2 and 51.3 m^2/g, respectively. They show a totally reversed trend of the crystallite size of SP powders (see Fig. 2). The smaller the crystallite size, the higher the measured specific surface area. Moreover, as shown in Fig. 6(b), the structure of the ZnO-added SP500 powder coating consisted of irregular nanocrystalline particles, which have a very high surface area. This may further provide the electrode structure with large active site areas and facilitate ionic transport during electrochemical faradaic reaction [5,25]. With the ZnO addition increased to 10 at%, the excess ZnO fails to provide enough valence changes in the electrode material, resulting in the decline in SC of the powder coating.

The electrochemical stability of the SP powder coatings was investigated by repeating CV test at a scan rate of 100 mV/s for 1200 cycles. Fig. 7 shows the long-term cycle

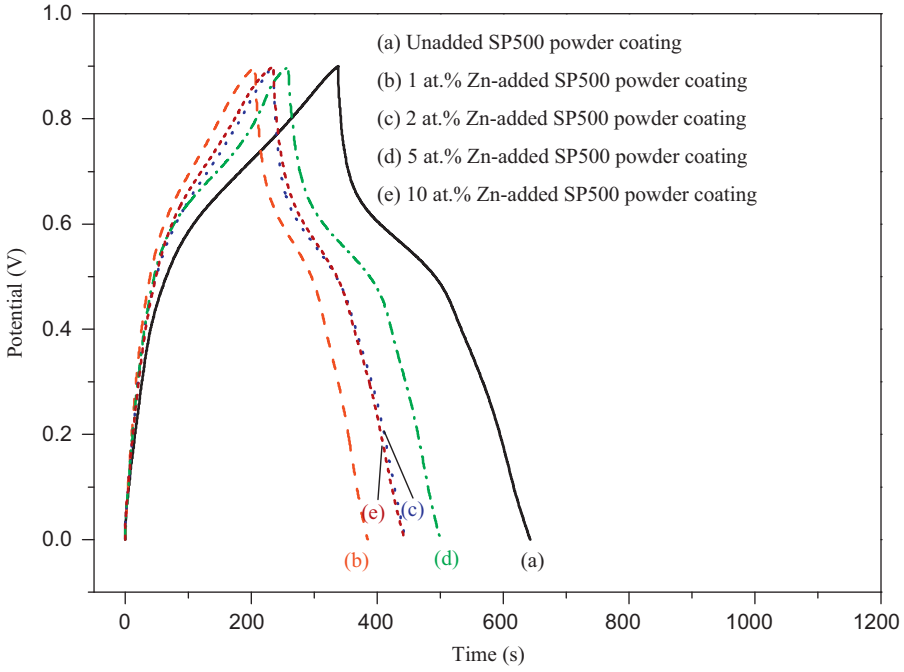

Fig. 5. Chronopotentiograms of Mn-oxide powder coatings measured at 1 mA between 0 and 0.9 V in 1.0 M Na_2SO_4 electrolyte as a function of ZnO addition.

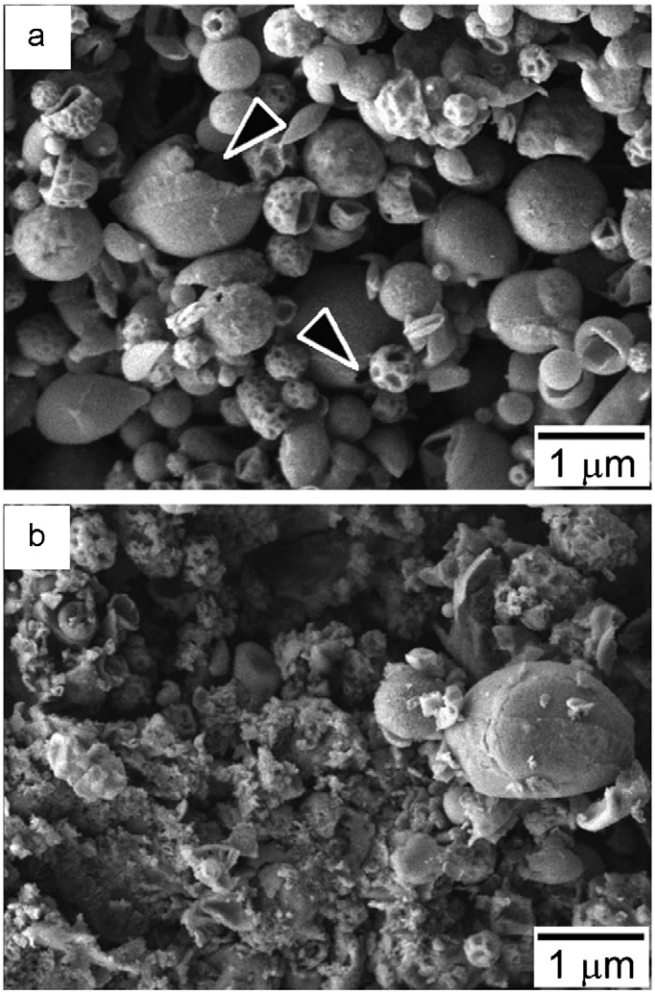

Fig. 6. SEM micrographs of electrophoretically deposited (a) unadded and (b) 5 at% ZnO-added SP500 Mn-oxide powder coatings before CV measurements.

performance of the unadded and ZnO-added SP500 Mn-oxide electrodes in 1.0 M Na_2SO_4 electrolyte. The capacitance of all the ZnO-added SP500 electrodes was higher than that of the unadded one. The SC of all the SP500 coatings increased dramatically after 50 cycles of CV, implying that surface of the coating was activated at the initial stage. After 50 cycles, SC declined gradually with increasing CV cycle number. The SC of the unadded SP500 coating declined rapidly after 200 CV cycles, and then it decreased slowly as the cycle number exceeded 1000. However, after the activation of the first 50 cycles, the capacitance of the ZnO-added coatings tended to decline slowly until the cycle number increased to 1200. Table 2 lists the maximum and minimum SCs of the SP500 powder coatings and their cycling efficiencies in the 1200-cycle life tests. The data indicate that the Zn addition can significantly improve the cycling stability of the EPD SP500 coatings to an efficiency higher than 90%. In other words, the ZnO-added EPD SP500 powder coatings are extremely efficient and have good electrochemical performance for supercapacitors.

The morphology of the EPD coatings was then observed using SEM due to their microstructural changes after CV tests. Fig. 8 shows the morphologies of the unadded and 5 at% ZnO-added SP500 particle coatings after the 1200-cycle CV measurements. As seen in Fig. 8(a), no obvious particulate morphology can be found on the surface of the coating. The surface is relatively smooth, with some traces of the collapsed particles. In our previous studies, we have demonstrated that the electrochemical reaction between particles and aqueous electrolyte tends to dissolve the particulate structure of the Mn-oxides during CV test [13,14]. Recalling the results of life tests shown in Fig. 7, the change in morphology caused by the repetitive

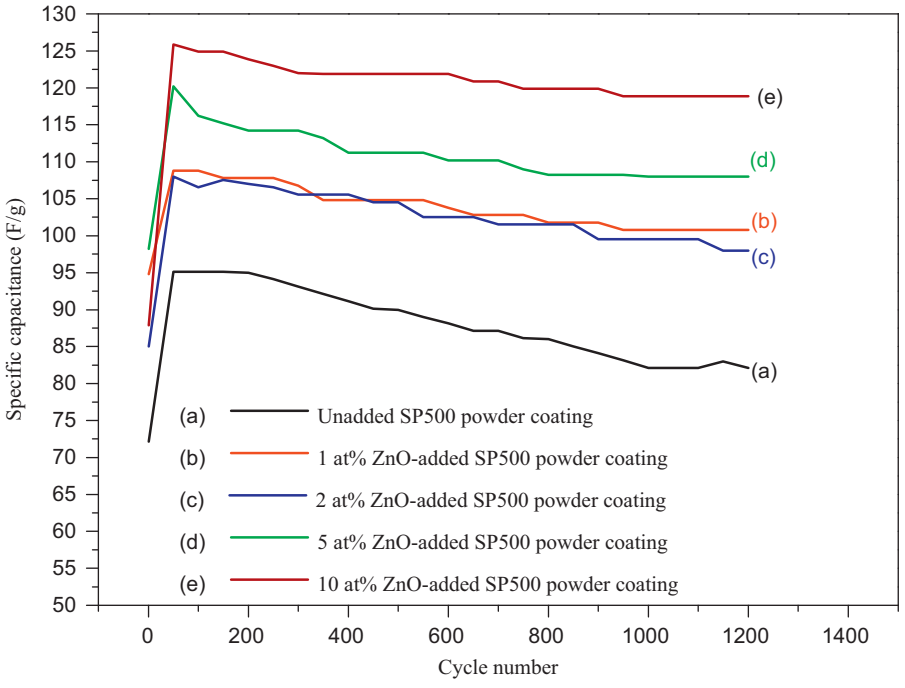

Fig. 7. Specific capacitance of SP500 Mn-oxide powder coatings with various amounts of ZnO addition measured in 1.0 M Na_2SO_4 electrolyte at a scan rate of 100 mV/s as a function of cycle number.

Table 2
Specific capacitance and cycling efficiency of SP500 powder coating in 1.0 M Na_2SO_4 at a scan rate of 100 mV/s as a function of ZnO addition during 1200 cycles of life test.

Specific capacitance (F/g)	ZnO addition in SP500 Mn-oxide powder (at%)				
	0	1	2	5	10
Maximum value	96	109	108	120	126
Minimum value	82	101	98	108	118
Cycling efficiency (%)	85.4	92.6	90.7	90.0	93.6

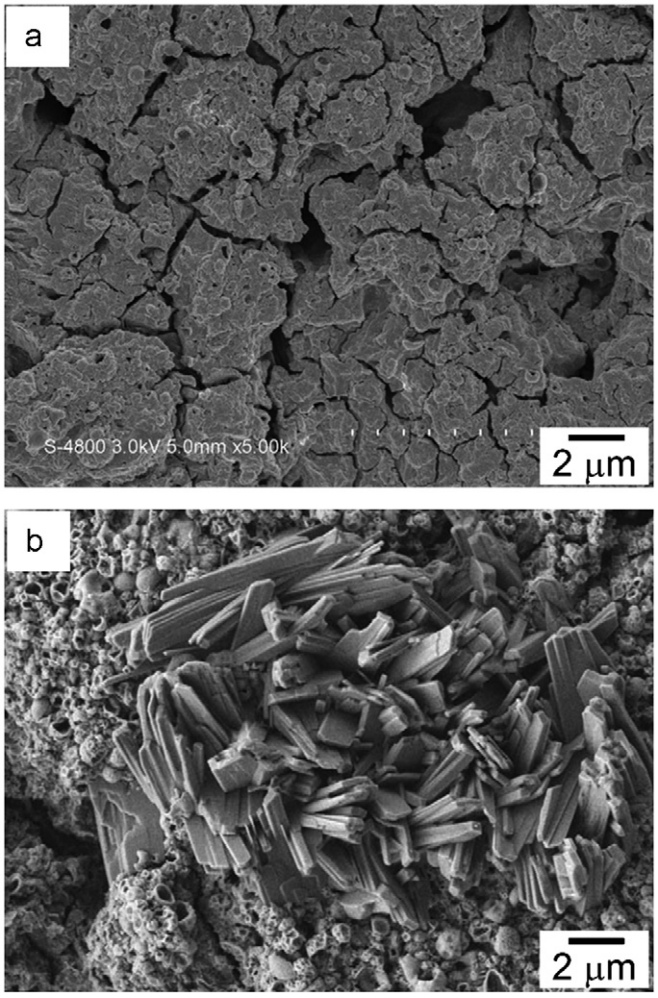

Fig. 8. SEM micrographs of (a) unadded and (b) 5 at% ZnO-added SP500 Mn-oxide powder coatings after life measurements.

dissolution-precipitation mechanism can be expected to cause a decline in SC of the EPD coating after the cyclic redox reactions. However, the morphology of the 5 at% ZnO-added SP500 coating is observably different from the unadded one after CV test. Some clusters of plate-like crystals can be observed on the surface of the CV-measured coating, except for the breakdown of the particulate Mn-oxide structure. The micrograph in Fig. 8(b) shows a magnified image of one of the clusters. Since the ZnO plates or rods can be prepared commonly by electrochemical deposition methods [26–28], such crystals are easily recognizable as precipitated ZnO in this system. Comparing this image with the morphology in Fig. 6(b), the growth of ZnO crystals is believed to occur via dissolution-precipitation during CV test.

Since the ionic radius of Zn^{2+} (0.74 Å, coordination number (CN)=6) is smaller than that of Mn^{2+} (0.83 Å, CN=6) and larger than that of Mn^{3+} (0.66 Å, CN=6), a nonstoichiometric homogeneous solid solution is expected to form in the as-pyrolyzed Mn-oxide matrix [21]. From the XRD data in Fig. 1, the SP500 powders were identified as Mn_3O_4 (the valence state of Mn is +2.67). The peak-shift of the Mn-oxide phase is noticed to increase as a function of ZnO addition. Recalling the result in Fig. 2, the lattice volume of SP500 powders was plotted as a function of ZnO addition. The lattice volume increases slightly from 0.3165 nm^3 for the unadded Mn-oxide to a value of 0.3175 nm^3 for the 1 at% ZnO-added Mn-oxide; then it subsequently decreases to 0.3114 nm^3 for the 10 at% ZnO-added equivalent. The expansion of the lattice volume may result from the formation of solid solution, facilitating ionic insertion/extraction during redox reaction and shortening the charging/discharging time. On the other hand, reduction in lattice volume suggests a possible formation of spinel-like phase, $Zn_xMn_{3-x}O_4$, due to the valence change from +2.67 to +3 [21]. This reduction in lattice volume will cause lattice distortion, which in turn reduces the size of the crystallites in the as-pyrolyzed particle. Subsequently, the Zn ions substituting for Mn ions may be extracted from the Mn_3O_4 lattice during the CV tests. Meanwhile, the SP Mn-oxide powder transforms into MnO_2 phase after CV [13], and insertion/extraction of Zn ions into/from MnO_2 is thus accompanied by the reversible reaction of Mn^{4+}/Mn^{3+} [29]. This physicochemical behavior may be a factor in the high cycling efficiency and stability of the ZnO-added SP500 powder coating. Furthermore, when the Zn-ion concentration on the surface of the coating is locally high enough to nucleate, the ZnO crystal has a tendency to grow via precipitation into a cluster structure, as shown in Fig. 8(b).

4. Conclusions

Nanocrystalline Mn-oxide powders with various ZnO additions have been synthesized from acetate-based salt precursors by spray pyrolysis at 500 °C. The resulting

powders are identified as Mn_3O_4 phase with a rounded particle shape and hollow structures. The crystallite size and specific surface area of SP Mn-oxide particles are decreased and increased, respectively, by additions of ≥ 2 at% ZnO. After EPD, the ZnO-added Mn-oxide powder coating exhibits a high specific capacitance of 230 F/g, which is an improvement of ~17% over that of the unadded one. Moreover, the composite powder coating exhibits a better physicochemical behavior of charge storage, revealing an extremely high cycling efficiency of higher than 90% after 1200 CV cycles.

Acknowledgment

This work was partially funded by the National Science Council of Taiwan (Grant nos. NSC 99-2221-E-035-032-MY3 and NSC 100-2628-E-035-002).

References

[1] B.E. Conway, Transition from supercapacitor to battery behavior in electrochemical energy storage, Journal of the Electrochemical Society 138 (1991) 1539–1548.
[2] S. Sarangapani, B.V. Tilak, C.P. Chen, Materials for electrochemical capacitors, Journal of the Electrochemical Society 143 (1996) 3791–3799.
[3] K.R. Prasad, N. Miura, Electrochemically synthesized MnO_2-based mixed oxides for high performance redox supercapacitors, Electrochemistry Communications 6 (2004) 1004–1008.
[4] C.Y. Lee, H.M. Tsai, H.J. Chuang, S.Y. Li, P. Lin, T.Y. Tseng, Characteristics and electrochemical performance of supercapacitors with manganese oxide-carbon nanotube nanocomposite electrodes, Journal of the Electrochemical Society 152 (2005) A716–A720.
[5] J.H. Jang, A. Kato, K. Machida, K. Naoi, Supercapacitor performance of hydrous ruthenium oxide electrodes prepared by electrophoretic deposition, Journal of the Electrochemical Society 153 (2006) A321–A328.
[6] J.P. Zheng, T.R. Jow, A new charge storage mechanism for electrochemical capacitors, Journal of the Electrochemical Society 142 (1995) L6–L8.
[7] J.P. Zheng, P.J. Cygan, T.R. Jow, Hydrous ruthenium oxide as an electrode material for electrochemical capacitors, Journal of the Electrochemical Society 142 (1995) 2699.
[8] H.Y. Lee, J.B. Goodenough, Supercapacitor behavior with KCl electrolyte, Journal of Solid State Chemistry 144 (1999) 220–223.
[9] S.-C. Pang, M.A. Anderson, T.W. Chapman, Novel electrode materials for thin-film ultracapacitors: comparison of electrochemical properties of sol–gel-derived and electrodeposited manganese dioxide, Journal of the Electrochemical Society 147 (2000) 444–450.
[10] H.Y. Lee, S.W. Kim, H.Y. Lee, Expansion of active site area and improvement of kinetic reversibility in electrochemical pseudocapacitor electrode, Electrochemical and Solid State Letters 4 (2001) A19–A22.
[11] C.-C. Hu, W.-C. Chen, K.-H. Chang, How to achieve maximum utilization of hydrous ruthenium oxide for supercapacitors, Journal of the Electrochemical Society 151 (2004) A281–A290.
[12] C.Y. Chen, C.K. Lin, Y.R. Lyu, H.H. Lin, W.H. Tuan, Pseudocapacitive manganese oxide prepared by a spray pyrolysis /electrostatic deposition technique, Advances in Science and Technolog 45 (2006) 1896–1901.
[13] C.-Y. Chen, Y.-R. Lyu, C.-Y. Su, H.-M. Lin, C.-K. Lin, Characterization of spray pyrolyzed manganese oxide powders deposited byelectrophoretic deposition technique, Surface and Coatings Technology 202 (2007) 1277–1281.
[14] S.C. Wang, C.Y. Chen, T.C. Chien, P.Y. Lee, C.K. Lin, Supercapacitive properties of spray pyrolyzed iron-added manganese oxidepowders deposited by electrophoretic deposition technique, Thin Solid Films 517 (2008) 1234–1238.
[15] K. Nomura, H. Ohta, K. Ueda, T. Kamiya, M. Hirano, H. Hosono, Thin-film transistor fabricated in single-crystalline transparent oxide semiconductor, Science 300 (2003) 1269–1272.
[16] T. Yoshida, D. Komatsu, N. Shimokawa, H. Minoura, Mechanism of cathodic electrodeposition of zinc oxide thin films from aqueous zinc nitrate baths, Thin Solid Films 451–452 (2004) 166–169.
[17] C.-Y. Tsay, K.-S. Fan, S.-H. Chen, C.-H. Tsai, Preparation and characterization of ZnO transparent semiconductor thin films by solgel method, Journal of Alloys and Compounds 4 (95) (2010) 126–130.
[18] M. Selvakumar, D. Krishna Bhat, A. Manish Aggarwal, S. Prahladh Iyer, G. Sravani, Nano ZnO-activated carbon composite electrodes for supercapacitors, Physica B 405 (2010) 2286–2289.
[19] D. Kalpana, K.S. Omkumar, S. Suresh., Kumar, N.G. Renganathan, A novel high power symmetric ZnO/carbon aerogel composite electrode for electrochemical supercapacitor, Electrochimica Acta 52 (2006) 1309–1315.
[20] Y. Zhang, X. Sun, L. Pan, H. Li, Z. Sun, C. Sun, B.K. Tay, Carbon nanotube-ZnO nanocomposite electrodes for supercapacitors, Solid State Ionics 180 (2009) 1525–1528.
[21] M.A. García, M.L. Ruiz-González, A. Quesada, J.L. Costa-Krämer, J.F. Fernández, S.J. Khatib, A. Wennberg, A.C. Caballero, M.S. Martín-González, M. Villegas, F. Briones, J.M. González-Calbet, A. Hernando, Interface double-exchange ferromagnetism in the Mn–Zn–O system: new class of biphase magnetism, Physical Review Letters 94 (2005) 217206.
[22] K. Tanaka, K. Fukui, S. Murai, K. Fujita, Room-temperature ferromagnetic phase in ZnO–MnO_2 system via solid-state reaction, Journal of Magnetism and Magnetic Materials 310 (2007) 2095–2096.
[23] C.-Y. Chen, Y.-R. Lyu, Effect of NiO addition on properties of bulk yttria-doped ceria sintered from their spray pyrolyzed powder, Ceramics International 38 (2012) 3291–3300.
[24] V. Subramanian, H. Zhu, R. Vajtai, P.M. Ajayan, B. Wei, Hydrothermal synthesis and pseudocapacitance properties of MnO_2 nanostructures, Journal of Physical Chemistry B 109 (2005) 20207–20214.
[25] N.-L. Wu, Nanocrystalline oxide supercapacitors, Materials Chemistry and Physics 75 (2002) 6–11.
[26] Y. Zhang, J. Mu, Controllable synthesis of flower- and rod-like ZnO nanostructures by simply tuning the ratio of sodium hydroxide to zinc acetate, Nanotechnology 18 (2007) 075606–075611.
[27] G.-R. Li, X.-H. Lu, D.-L. Qu, C.-Z. Yao, F.-L. Zheng, Q. Bu, C.-R. Dawa, Y.-X. Tong, Electrochemical growth and control of ZnO dendritic structures, Journal of Physical Chemistry C 111 (2007) 6678–6683.
[28] M. Chang, X. Cao, H. Zeng, Electrodeposition growth of vertical ZnO nanorod/polyaniline heterostructured films and their optical properties, Journal of Physical Chemistry C 113 (2009) 15544–15547.
[29] C. Xu, H. Du, B. Li, F. Kang, Y. Zeng, Reversible insertion properties of zinc ion into manganese dioxide and its application for energy storage, Electrochemical and Solid-State Letters 12 (2009) A61–A65.